

MicroRNA-139-5p negatively regulates NME1 expression in hepatocellular carcinoma cells

Jun Yang^{1,B,C,E,F}, De Zhi Li^{2,B,D,F}, Yu Pang^{3,B,D,F}, Tao Zhou^{2,B,D,F}, Jia Sun^{2,4,B,D,F}, Xian Yi Cheng^{3,B,D,F}, Wei V. Zheng^{2,A,E,F}

¹ Department of Radiology, Peking University Shenzhen Hospital, China

² Intervention and Cell Therapy Center, Peking University Shenzhen Hospital, China

³ Department of Minimally Invasive Intervention, Peking University Shenzhen Hospital, China

⁴ Shenzhen Beike Biotechnology Research Institute, China

A – research concept and design; B – collection and/or assembly of data; C – data analysis and interpretation;

D – writing the article; E – critical revision of the article; F – final approval of the article

Advances in Clinical and Experimental Medicine, ISSN 1899–5276 (print), ISSN 2451–2680 (online)

Adv Clin Exp Med. 2022;31(6):655–670

Address for correspondence

Wei V. Zheng

E-mail: zhengw2013@yeah.net

Funding sources

This work was supported by grants from the Sanming Project of Medicine in Shenzhen (grant No. SZSM201612071), the Cell Technology Center and Transformation Base, Innovation Center of Guangdong-Hong Kong-Macao Greater Bay Area, Ministry of Science and Technology of China (grant No. YCZYPT [2018]03-1), and Shenzhen Key Discipline of Stem Cell Clinical Research, the Key Medical Disciplines Construction Funding in Shenzhen (grant No. SZXK078).

Conflict of interest

None declared

Received on November 16, 2021

Reviewed on January 20, 2022

Accepted on February 10, 2022

Published online on April 19, 2022

Cite as

Yang J, Li DZ, Pang Y, et al. MicroRNA-139-5p negatively regulates NME1 expression in hepatocellular carcinoma cells. *Adv Clin Exp Med.* 2022;31(6):655–670. doi:10.17219/acem/146579

DOI

10.17219/acem/146579

Copyright

Copyright by Author(s)

This is an article distributed under the terms of the Creative Commons Attribution 3.0 Unported (CC BY 3.0) (<https://creativecommons.org/licenses/by/3.0/>)

Abstract

Background. High expression of NME1 is associated with hepatocellular carcinoma (HCC) progression and poor prognosis. However, there are few reports on the association between NME1 and microRNAs (miRNAs) in HCC progression.

Objectives. To explore miRNAs that regulate NME1 expression in HCC.

Materials and methods. Data from the Cancer Genome Atlas (TCGA), Human Protein Atlas (HPA), TargetScan, starBase, and mirDIP were used to analyze the expression pattern of NME1 in HCC tissues, the relationship between NME1 level and the progression of HCC or patient prognosis, miRNAs targeting NME1, and the biological processes that may be regulated by NME1. The regulation of miRNAs to NME1 was assessed using the dual-luciferase reporter assay, quantitative reverse transcription polymerase chain reaction (qRT-PCR) and western blotting. The cell cycle and cell proliferation were detected using propidium iodide (PI) staining and EdU assay, respectively.

Results. Highly expressed NME1 in HCC was associated with HCC progression and prognosis. The miR-139-5p and miR-335-5p were weakly expressed in HCC samples and negatively correlated with NME1. The down-regulation of miR-139-5p in HCC patients resulted in worse overall survival (OS) and disease-free interval (DFI); however, the level of miR-335-5p was not significantly correlated with OS and DFI in patients with HCC. In vitro experiments verified that the level of miR-139-5p was lower and NME1 expression was higher in HCC cell lines compared to L-02. Moreover, miR-139-5p negatively regulates the expression of NME1 in HCC cell lines. The NME1 may regulate cell cycle, DNA replication, oxidative phosphorylation, and the pentose phosphate pathway. The miR-139-5p inhibited cell proliferation by negatively regulating NME1 expression.

Conclusions. The upregulation of NME1 in HCC indicates a poor prognosis. The NME1 is negatively regulated by miR-139-5p to inhibit cell proliferation.

Key words: microRNA, hepatocellular carcinoma, bioinformatics analysis, NME1

Background

Hepatocellular carcinoma (HCC) has become the second deadliest cancer-related factor globally.¹ The occurrence of liver cancer depends on the complex interaction between genetic susceptibility factors, environmental factors, carcinogens, and viral exposure.² Importantly, recent studies suggest that some single nucleotide polymorphisms (SNPs) are associated with HCC development and clinical outcomes.^{3,4}

The *NME1*, also known as *NDPK-A* and *NM23-H1*, is located on chromosome 17q21.^{5,6} The *NME1* contains an arginine–glycine–asparagine (RGD) sequence, which is a ligand that exists in a variety of adhesive protein molecules that specifically bind to integrin receptors, participate in the polymerization of cytoskeleton protein microfilaments, and maintain cell stability and directional cell migration.^{7–9} Moreover, *NME1* functions as a histidine kinase, nucleoside-diphosphate kinase and 3′-5′ exonuclease, and plays an essential role in cellular proliferation, embryonic development, differentiation, and transcriptional regulation.^{7,10,11} The expression of the *NME1* mRNA is reduced in cells with high metastatic ability.⁴ Many reports have demonstrated that *NME1* plays an essential role in the growth and metastasis of various cancers such as breast cancer, non-small cell lung cancer and ovarian cancer.^{4,12–14}

MicroRNAs (miRNAs) are common noncoding small molecular RNAs. The miRNAs bind to the 3′ untranslated region (UTR) of targeting mRNAs to regulate the translation and degradation of mRNAs, thus participating in gene expression, ontogenesis and disease occurrence.^{8,15,16} In breast cancer cells, *NME1* is regulated by miR-146a and it promotes cell growth and invasion.⁸ In colorectal cancer cells, increased miR-28-3p downregulates the level of *NME1*, inhibiting cell growth and metastasis.¹⁷ Furthermore, 1 study showed that the upregulated *NME1* in HCC tissues contribute to the advancing progression and poor prognosis of patients with HCC.¹⁸ However, there are few studies about the regulation of miRNA on *NME1* in HCC.

Objectives

In this study, we aimed to investigate the relationship between miRNAs and *NME1*, and uncover the effect of miRNAs/*NME1* axis on the progression of HCC.

Materials and methods

Data from the Cancer Genome Atlas database

The mRNA-seq, miRNA-seq and clinical data of Cancer Genome Atlas-Liver Hepatocellular Carcinoma (TCGA-LIHC) were obtained from the University of California,

Santa Cruz (UCSC) Xena website (<https://tcga.xenahubs.net>) and Genomic Data Commons (GDC) website (<https://portal.gdc.cancer.gov/>). The data contained 369 samples of HCC tissues and 50 samples of adjacent normal tissues. Out of the 369 HCC samples, 339 with follow-up information were included in the discovery dataset. With respect to the HCC stage, 170 out of 339 samples were in stage I, 84 out of 339 were in stage II, 81 out of 339 were in stage III, and 4 out of 339 were in stage IV (Table 1).

Data from the Human Protein Atlas database

To compare the difference in protein levels of *NME1* between normal liver tissues and HCC tissues, we obtained data on immunohistochemistry (IHC) staining that detected *NME1*, from the Human Protein Atlas (HPA) database (<https://www.proteinatlas.org/>). According to the previous description,¹⁹ the protein expression score was defined as not detected for samples with <25% stained cells and negative or weak staining intensity; the protein expression score was defined as low for samples with 25–75% stained cells and weak staining intensity, or with <25% stained cells and moderate staining intensity; the protein expression score was defined as medium for samples with 25–75% stained cells or >75% stained cells and moderate staining intensity, or with <25% stained cells and intense staining; the protein expression score was defined as high for samples with 25–75% or >75% stained cells and strong staining intensity.

Prediction of miRNAs targeting NME1

We used TargetHumanScan (http://www.targetscan.org/vert_80/), starBase (<https://starbase.sysu.edu.cn/>) and mirDIP (<http://ophid.utoronto.ca/mirDIP/>) databases to screen the miRNAs targeting *NME1*. The miRNAs downregulated (log2 multiple change <0) in TCGA-LIHC were also screened out. Based on the aforementioned screening, the Venn diagram was drawn, using TBtools v. 1.082 (<https://github.com/CJ-Chen/TBtools/releases>). Two miRNAs at the intersection of the Venn diagram were used for further study.

Cell culture

The L-02 cells are normal hepatocytes. The Hep3B cells are HCC cells and contain an integrated hepatitis B virus (HBV) genome. The Huh-7 is derived from liver tissue from a Japanese man with highly differentiated HCC and does not contain the HBV genome. The HepG2 is derived from the hepatic tissue of a 15-year-old American male who has hepatoblastoma, and does not contain HBV genome. The Hep3B, Huh7 and HepG2 are representatives of HCC and carry high-risk metastatic property. The SMMC-7721 is derived from a Chinese man. The L-02, Hep3B, HepG2,

Table 1. Correlation between clinicopathological variables and NME1 mRNA expression level in hepatocellular carcinoma (HCC)

Variables	NME1 expression			p-value ^a
	total	high	low	
	(n = 339)	(n = 105)	(n = 234)	
Age [years]				
<65	208 (61.4%)	68 (64.8%)	140 (59.8%)	0.458
≥65	131 (38.6%)	37 (35.2%)	94 (40.2%)	
Gender				
Male	231 (68.1%)	79 (75.2%)	152 (65.0%)	0.0797
Female	108 (31.9%)	26 (24.8%)	82 (35.0%)	
Family history of cancer				
No	196 (57.8%)	67 (63.8%)	129 (55.1%)	0.301
Yes	98 (28.9%)	25 (23.8%)	73 (31.2%)	
Unknown	45 (13.3%)	13 (12.4%)	32 (13.7%)	
TNM stage				
I	170 (50.1%)	43 (41.0%)	127 (54.3%)	0.138
II	84 (24.8%)	30 (28.6%)	54 (23.1%)	
III	81 (23.9%)	30 (28.6%)	51 (21.8%)	
IV	4 (1.2%)	2 (1.9%)	2 (0.9%)	
Histologic grade				
G1–G2	212 (62.5%)	56 (53.3%)	156 (66.7%)	0.0315
G3–G4	125 (36.9%)	49 (46.7%)	76 (32.5%)	
Unknown	2 (0.6%)	0 (0%)	2 (0.9%)	
Ishak score				
0–4	124 (36.6%)	42 (40.0%)	82 (35.0%)	0.237
5–6	74 (21.8%)	17 (16.2%)	57 (24.4%)	
Unknown	141 (41.6%)	46 (43.8%)	95 (40.6%)	
Child–Pugh grade				
A	207 (61.1%)	71 (67.6%)	136 (58.1%)	0.247
B–C	21 (6.2%)	5 (4.8%)	16 (6.8%)	
Unknown	111 (32.7%)	29 (27.6%)	82 (35.0%)	
Vascular invasion				
None	193 (56.9%)	49 (46.7%)	144 (61.5%)	0.0166
Micro	84 (24.8%)	27 (25.7%)	57 (24.4%)	
Macro	14 (4.1%)	6 (5.7%)	8 (3.4%)	
Unknown	48 (14.2%)	23 (21.9%)	25 (10.7%)	
Alpha fetoprotein				
Negative	143 (42.2%)	40 (38.1%)	103 (44.0%)	0.593
Positive	120 (35.4%)	40 (38.1%)	80 (34.2%)	
Unknown	76 (22.4%)	25 (23.8%)	51 (21.8%)	
Residual tumor				
R0	301 (88.8%)	93 (88.6%)	208 (88.9%)	0.656
R1–R2	12 (3.5%)	5 (4.8%)	7 (3.0%)	
Unknown	26 (7.7%)	7 (6.7%)	19 (8.1%)	
Living status				
Alive	224 (66.1%)	59 (56.2%)	165 (70.5%)	0.0142
Dead	115 (33.9%)	46 (43.8%)	69 (29.5%)	
Disease status				
No	163 (48.1%)	45 (42.9%)	118 (50.4%)	0.405
Yes	132 (38.9%)	46 (43.8%)	86 (36.8%)	
Unknown	44 (13.0%)	14 (13.3%)	30 (12.8%)	

^a χ^2 test. Values in bold are statistically significant.

SMMC-7721, and Huh7 (cat. No. IM-H289, IM-H367, IM-H038, IM-H047, and IM-H040, respectively; Immocell, Xiamen, China) were maintained in Dulbecco's modified Eagle medium (DMEM; cat. No. D0819; Sigma-Aldrich, St. Louis, USA) with 10% fetal bovine serum (FBS; cat. No. 12483020; Gibco, Detroit, USA), 100 U/mL penicillin, and 100 U/mL streptomycin (cat. No. 15070063; Gibco) at 37°C.

Plasmids and mimic

The 3' UTR of *NME1* gene was amplified from genomic DNA of Hep3B cells using polymerase chain reaction (PCR). The primers were shown in Table 2. The *NME1* 3' UTR fragment was cloned into the pmirGLO Vector (Antihela, Xiamen, China) downstream to the firefly luciferase reporter gene. Mutant *NME1* 3' UTR (3' UTR MUT) was

generated from the wide-type *NME1* 3' UTR (3' UTR WT) using the Mut Express II Fast Mutagenesis Kit V2 (cat. No. C214-1; Vazyme, Nanjing, China).

The plv-CMV-mcs-PGK-puro vector (Antihela) was used to overexpress NME1, named NME1 OE plasmid. The blank vector was used as a negative control. The primers for the construction of NME1 OE plasmid were shown in Table 2.

The mimic NC (ID: miR1N0000001-1-5), miR-139-5p mimic (ID: miR10000250-1-5), inhibitor NC (miR2N0000001-1-5), and miR-139-5p inhibitor (ID: miR20000250-1-5), whose sequences are shown in Table 3, were purchased from RiboBio (Guangzhou, China).

Dual-luciferase reporter assay

The Hep3B and Huh7 cells (3×10^5 /well) were seeded into the 24-well plates. Twelve hours later, the cells were co-transfected with 200 pmol/well mimic NC or miR-139-5p mimic, and 1 µg/well 3' UTR WT or MUT plasmid using Lipofectamine 2000 (cat. No. 11668027; Invitrogen, Carlsbad, USA). After a 24-hour transfection, the luciferase activities of Hep3B and Huh7 cells were detected using The Dual-Luciferase® Reporter Assays System (cat. No. E1910; Promega, Madison, USA). The firefly luciferase activities were calibrated to Renilla luciferase activities. Each detection was performed in triplicate.

Transfection

The Hep3B and Huh7 cells (2×10^6 /well) were seeded into the 6-well plates. Twelve hours later, 800 pmol/well miR-139-5p mimic, miR-139-5p inhibitor or corresponding negative control was co-transfected into Hep3B and Huh7 cells with or without 4 µg of Vector or NME1 OE plasmid using Lipofectamine 2000. After the incubation for 24–48 h, Hep3B and Huh7 cells were harvested and

subjected to the analyses of quantitative reverse transcription polymerase chain reaction (qRT-PCR), western blotting, cell cycle, and cell proliferation.

qRT-PCR

After treatment, the total RNA was extracted from Huh7 and Hep3B cells using Total RNA Extraction Reagent (cat. No. R401-01; Vazyme, Nanjing, China.). The cDNA of NEM1 was synthesized from 1 µg of total RNA using HiScript II One Step RT-PCR Kit (cat. No. P611-01; Vazyme). The transcription reaction of miR-139-5p was performed using 1 µg of total RNA with the miRNA 1st Strand cDNA Synthesis Kit (cat. No. MR101-01; Vazyme). The qPCR was performed using an iQ5 real-time PCR detection system (Bio-Rad Laboratories, Hercules, USA) with a ChamQ Universal SYBR® qPCR Master Mix kit (cat. No. Q311-02, Vazyme). The thermocycling conditions were: 96°C for 5 min, followed by 42 cycles at 96°C for 25 s, 58°C for 30 s and 72°C for 25 s. Expression levels were measured using the $2^{-\Delta\Delta C_t}$ method and normalized to those of U6 or 18s rRNA. The primers for reverse transcription and qPCR are shown in Table 4.

Western blotting

After treatment, the total protein was extracted from Huh7 and Hep3B cells using RIPA lysis solution. Subsequently, the BCA protein concentration determination kit (cat. No. P0012S; Beyotime, Shanghai, China) was used to quantify total protein. Samples (12 µg/lane) were loaded for electrophoresis on 10% denaturing sodium dodecyl sulfate-polyacrylamide gel electrophoresis (SDS-PAGE) gels. Western blotting was performed as previously described.²⁰ The following primary antibodies were used: anti-NME1 (cat. No. 11086-2-AP, 1:500; Proteintech, Wuhan, China) and anti-GAPDH (cat. No. 10494-1-AP, 1:5000;

Table 2. The primers for plasmid construction

Name	Sequence 5'-3'
3' UTR WT-F	GCTCGCTAGCCTCGAGCTGTAGGAAATCTAGTTATTTACAG
3' UTR WT-R	ATGCCTGCAGGTCGACTGTATGTGAGACCTCAAAATAATC
3' UTR MUT-F	GCTCGCTAGCCTCGAGGAAATCTAGTTATTTACAGGAACCTC
NME1-F	GCGTGC GGCTGCCACCATGGCCAACTGTGAGCGTAC
NME1-R	TCTAGGGATCCGGGCCCTCATTCATAGATCCAGTTC

F – forward primer; R – reverse primer; UTR – untranslated region; 3' UTR WT – wide-type *NME1* 3' UTR; 3' UTR MUT – mutant *NME1* 3' UTR.

Table 3. The sequences of miR-139-5p mimic and inhibitor

Name	Sequence 5'-3'
mimic NC	UCUACAGUGCAGUGUCUCCAGU
miR-139-5p mimic	UCUACAGUGCAGUGUCUCCAGU
inhibitor NC	CAGUACUUUUGUGUAGUACAA
miR-139-5p inhibitor	ACUGGAGACACGUGCAGUGUAGA

Table 4. The primers for quantitative reverse transcription polymerase chain reaction (qRT-PCR)

Name	Sequence 5'-3'
miR-139-5p RT	GTCGTATCCAGTGCAGGGTCCGAGGTATTCGCACTGGATACGACACTGGA
miR-139-5p-QF	CGCGTCTACAGTGCACGTGTC
miR-139-5p-QR	AGTGCAGGGTCCGAGGTATT
U6-QF	CTCGCTTCGGCAGCACA
U6-QR	AACGCTTCACGAATTTGCGT
NME1-QF	ACCATCCGTGGAGACTTCTGCA
NME1-QR	ACCAGTTCCTCAGGGTGAAACC
18s rRNA-QF	ACCCGTTGAACCCATTCGTGA
18s rRNA-QR	GCCTCACTAAACCATCCAATCGG

QF – forward primer for (qRT-PCR); QR – reverse primer for qRT-PCR; RT – reverse transcription.

Proteintech). The secondary antibody was horseradish peroxidase (HRP)-conjugated goat anti-rabbit IgG (cat. No. SA00001-2, 1:2000; Proteintech). The quantification by densitometry was performed using ImageJ 1.52v (National Institutes of Health, Bethesda, USA). The *GAPDH* was used as an internal control.

Cell cycle assay

After transfection for 48 h, Huh7 and Hep3B cells were fixed using 70% ethanol at -20°C for 6 h. The fixed cells were then treated with 0.5% Triton X-100 and 15 $\mu\text{g}/\text{mL}$ RNase at 37°C for 30 min. Subsequently, the fixed cells were stained with 15 $\mu\text{g}/\text{mL}$ propidium iodide (PI) at 28°C for 30 min. After staining, the cells were subjected to a flow cytometer NovoCyte 1300 (ACEA Biosciences Inc., Hangzhou, China) for analysis.

Cell proliferation assay

After a 24-hour transfection, Huh7 and Hep3B cells were seeded in wells of 96-well plates. Twenty-four hours later, the proliferation of cells was detected using Cell-Light EdU Apollo 488 In Vitro Kit (cat. No. C10310-3; RiboBio) according to the manufacturer's instructions. The nucleus was stained using 10 $\mu\text{g}/\text{mL}$ 4',6-diamidino-2-phenylindole (cat. No. C1002, DAPI; Beyotime). Images were photographed using a fluorescent microscope (MOTIC, Hong Kong, China). The ImageJ software was used to count cell number.

Statistical analyses

The edgeR package v. 3.30.3 (<http://www.bioconductor.org/packages/release/bioc/html/edgeR.html>) in R was used to: analyze the divergent levels of NME1 mRNA, miR-335-5p and miR-139-5p between normal liver tissues and HCC tissues; and analyze the correlation of NME1 mRNA level with clinicopathological variables, miR-335-5p level and miR-139-5p level. Receiver operating characteristic (ROC) curve was used to judge the diagnostic value

of NME1 in HCC, and the area under the curve (AUC) was calculated using ROC package v. 1.0-11 (<http://ipatys.github.io/ROCR/>). The Kaplan–Meier survival curves were plotted using the R survival package v. 3.1-12 (<https://github.com/therneau/survival>). Gene set enrichment analysis (GSEA) was executed using GSEA software v. 4.0.0 (<http://www.gsea-msigdb.org/>). The proportionality of hazard function was checked based on the Schoenfeld residuals. The IBM SPSS software v. 21.0. (IBM Corp., Armonk, USA) was used to perform statistical analysis of our experimental data. Data are presented as mean \pm standard deviation (SD). The Shapiro–Wilk test was performed to determine whether the data follow a normal distribution. The Levene's test was used to ensure the homogeneity of variance. The Mann–Whitney test was performed to compare the difference between the 2 groups of non-parametric data. The Kruskal–Wallis one-way analysis of variance (ANOVA) followed by Dunn's multiple comparison test were used for 3 or more groups of nonparametric data. The survival curves were calculated using the Kaplan–Meier method, and the significance was determined using the log-rank test. The Student's t-test was performed to compare the difference between 2 groups of parametric data. The ANOVA followed by the Tukey's post hoc test was used for multiple comparisons among 3 or more groups of parametric data. The value of $p < 0.0500$ was considered statistically significant.

Results

NME1 is highly expressed in HCC tissues

Gene Expression Profiling Interactive Analysis (GEPIA) was used to review the mRNA levels of NME1 in different carcinomas and corresponding normal tissues adjacent to cancer. In most healthy organs of the human body, the mRNA level of NME1 was particularly low (Fig. 1A). The NME1 mRNA levels in HCC tissues ($n = 369$) from TCGA were significantly higher than those in the healthy liver ($n = 50$) (Fig. 1B, $p < 0.0001$). The ROC curve also

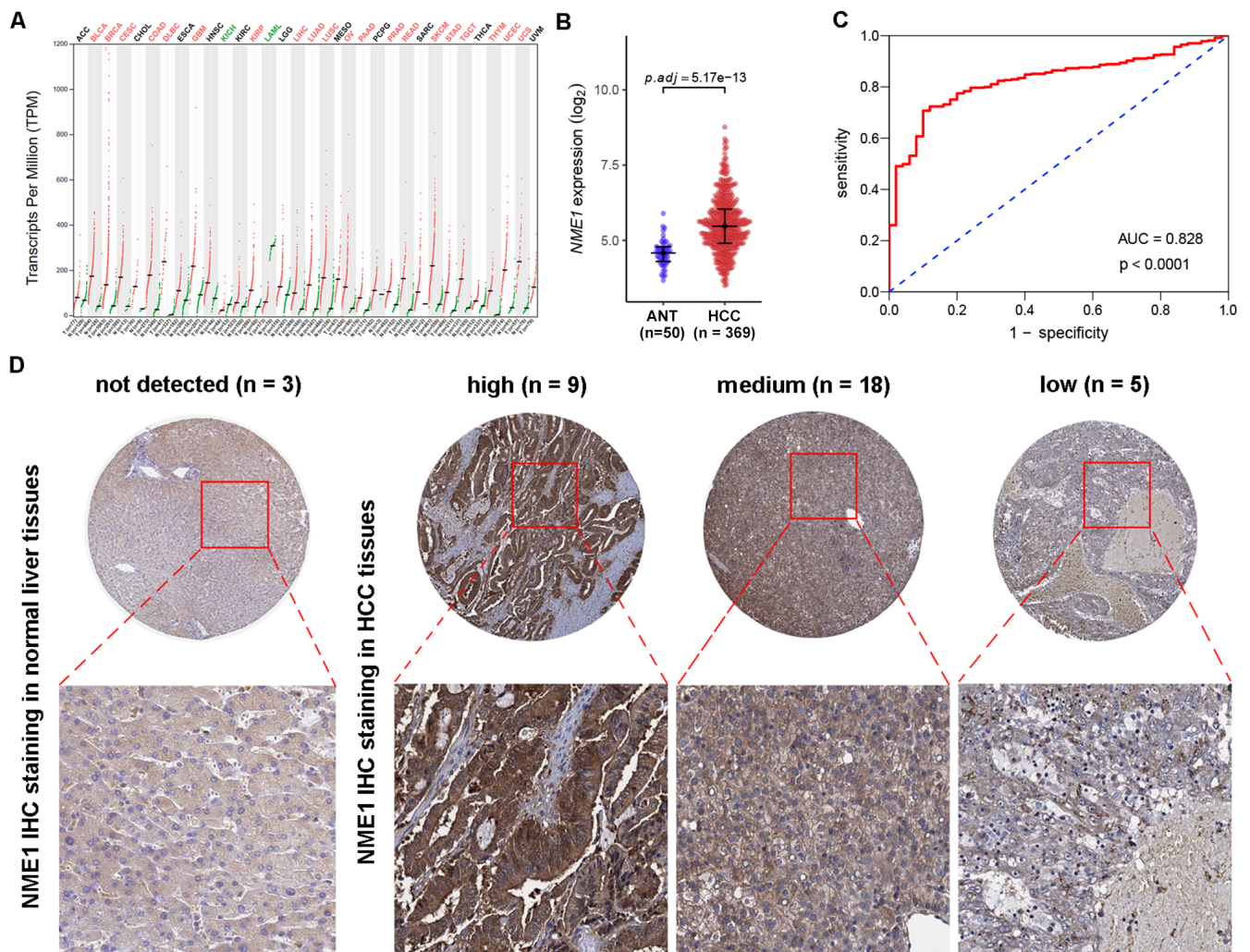


Fig. 1. The expression of NME1 is upregulated in hepatocellular carcinoma (HCC). A. mRNA levels of NME1 in different tumor tissues and normal tissues (ANT) from Gene Expression Profiling Interactive Analysis (GEPIA); B. The difference of NME1 mRNA level between HCC tissues ($n = 369$) and ANT ($n = 50$) from the Cancer Genome Atlas (TCGA); C. The receiver operating characteristic (ROC) curve was used to verify the diagnostic value of NME1 upregulation for HCC; D. Immunohistochemistry images of NME1 in normal liver tissues and HCC tissues from Human Protein Atlas (HPA). The Mann–Whitney test was used to analyze the data (A,B)

AUC – area under the curve; IHC – immunohistochemistry.

confirmed that elevated NME1 was valuable for the diagnosis of HCC (Fig. 1C, $AUC = 0.828$, $p < 0.0001$). Moreover, immunohistochemical staining data from the HPA database were downloaded to study the protein level of NME1 in HCC tissues and normal liver tissues. The NME1 staining was the weakest in normal liver tissues, and was high (9/32), moderate (18/32), or low (5/32) in the cytoplasm of a high proportion of HCC tissues (Fig. 1D). These data indicated that NME1 is highly expressed in HCC tissues.

NME1 overexpression is correlated with HCC progression

Next, we divided patients from TCGA into different subgroups and compared the mRNA levels of NME1. Patients with alpha-fetoprotein positivity ($n = 120$) had higher NME1 transcriptional expression than patients who were alpha-fetoprotein-negative ($n = 143$) (Fig. 2A, $p < 0.0100$).

The NME1 transcription levels were higher in patients with histologic grade 3 HCC ($n = 113$) than in patients with histologic grade 1 ($n = 46$, $p < 0.0500$) or grade 2 ($n = 166$, $p < 0.0500$) HCC (Fig. 2B). There was no significance in the relationship between increased NME1 expression and Child–Pugh grade in HCC patients (Fig. 2C, $n = 228$, $p > 0.0500$). The NME1 mRNA level in deceased patients with HCC ($n = 224$) was higher than that in living HCC patients ($n = 115$) (Fig. 2D, $p < 0.0100$). The NME1 mRNA level in patients with HCC TNM stage II ($n = 84$, $p < 0.0500$) or III ($n = 81$, $p < 0.0100$) was higher than of patients with HCC TNM stage I ($n = 170$) (Fig. 2E). The NME1 expression was higher in HCC tissue with microvascular infiltration ($n = 84$) than in HCC tissue without vascular infiltration ($n = 193$, $p < 0.0100$) (Fig. 2F). The correlation of NME1 mRNA level with clinicopathological variables was summarized in Table 1. These findings indicate that elevated NME1 is associated with HCC progression.

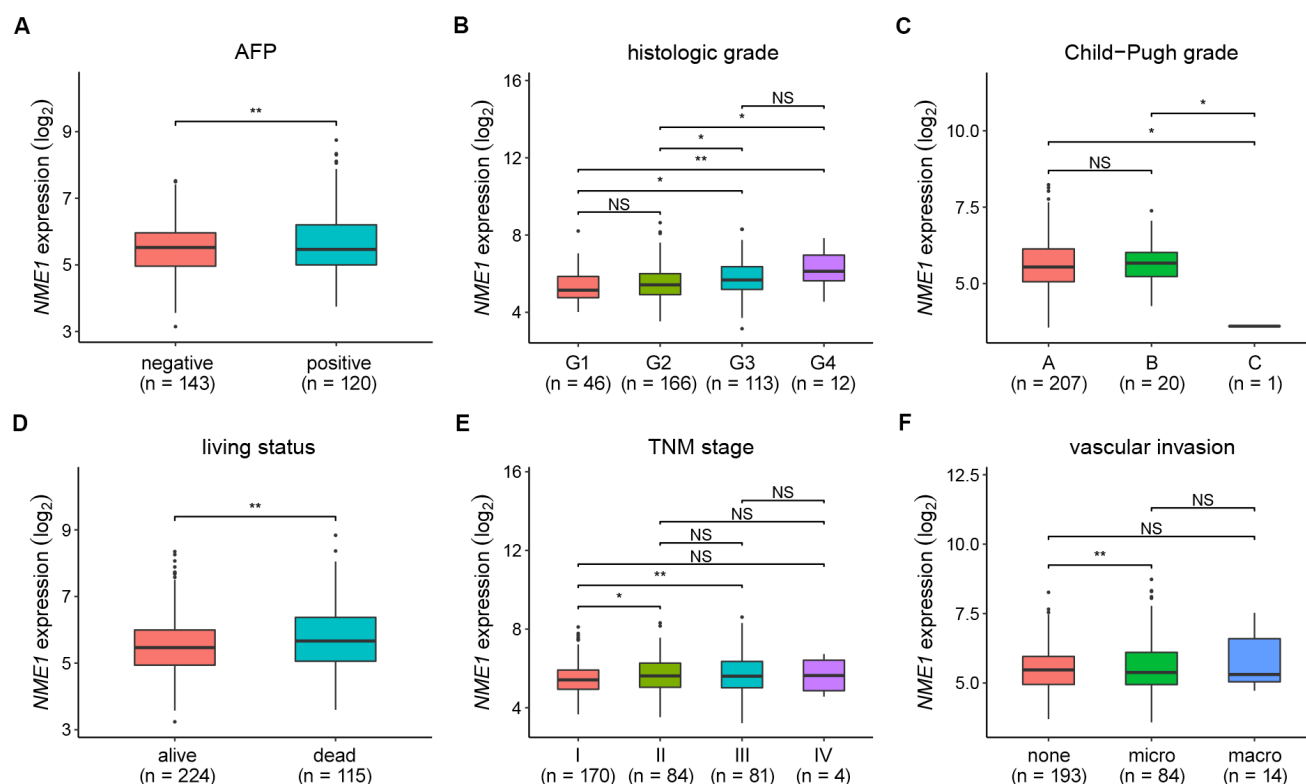


Fig. 2. The NME1 overexpression is correlated with hepatocellular carcinoma (HCC) progression. Patients from the Cancer Genome Atlas (TCGA) were grouped according to serum alpha fetoprotein (AFP) expression levels (A), histological grade (B), Child–Pugh grade (C), living status (D), TNM stages (E), and vascular invasion (F), and NME1 mRNA levels in different groups were analyzed. The Mann–Whitney test was used to analyze the data (A–F)

NS – no significance; * $p < 0.0500$; ** $p < 0.0100$.

Kaplan–Meier curve and nomogram verify the prognostic value of NME1 in HCC

Analyzing the Kaplan–Meier curve drawn using data from TCGA, we found that high NME1 mRNA level was significantly correlated with poor overall survival (OS) ($n = 339$, $p = 0.0067$) and disease-free interval (DFI) ($n = 295$, $p = 0.0120$) (Fig. 3A,B). Moreover, among patients with TNM stage III or IV HCC, the OS of patients with high NME1 transcription levels was poorer than that of those with low NME1 transcription levels ($n = 85$, $p = 0.0420$). The relationship between DFI of patients with TNM stage III or IV of HCC and NME1 transcription levels was not significant ($n = 68$, $p = 0.0610$) (Fig. 3C,D). In general, high NME1 mRNA level was associated with poor OS or DFI. The following nomogram and the calibration curve confirmed that the predicted survival probabilities were in excellent agreement with the actual observed survival probabilities (1-, 3-, and 5-year OS and DFI) (Fig. 4). Together, the level of NME1 mRNA is valuable to evaluate the prognosis of HCC.

miR-139-5p negatively regulates NME1

The Venn diagram showed that miR-139-5p and miR-335-5p may target to the 3' UTR of NME1 (Fig. 5A, Supplementary Table 1 available at <https://doi.org/10.5281/>

zenodo.6131676). The TCGA-LIHC data showed that the levels of hsa-miR-139-5p ($p < 0.0001$) and hsa-miR-335-5p ($p < 0.0001$) in HCC tissues were lower than those in normal adjacent tissues, and were negatively correlated with the mRNA level of NME1 (Fig. 5B–E). Moreover, the Kaplan–Meier curve showed that HCC patients with lower miR-139-5p level had poorer OS ($n = 367$, $p < 0.0001$) and DFI ($n = 314$, $p < 0.0001$), while there was no significance in the correlation of miR-335-5p levels with OS ($n = 364$, $p = 0.2280$) or DFI ($n = 314$, $p = 0.0610$) in HCC patients (Fig. 5F–I). These data suggested that miR-139-5p may interact with NME1 3' UTR. Next, we performed in vitro experiments to verify this hypothesis. As shown in Fig. 6A, the overexpression of miR-139-3p decreased the luciferase activity in Hep3B and Huh7 cells, which was abolished by the mutation of 3' UTR of NME1. These results suggested that miR-139-5p targets NME1. The expression levels of miR-139-5p and NME1 in HCC cell lines (SMMC-7721, Huh7, HepG2, and Hep3B) and normal liver cell line (L-02) were detected. The results showed that the expression levels of miR-139-5p and NME1 in HCC cell lines were higher than those in L-02 (Fig. 6B–D, $n = 3$, all $p < 0.0500$). Moreover, Hep3B and Huh7 cells had the highest NME1 level and the lowest miR-139-5p level. Therefore, these 2 cells were chosen for in vitro experiments. In addition, the miR-139-5p overexpression elevated the levels of miR-139-5p in HCC cells (Hep3B: 1.015 ± 0.2227 fold compared to 6.007 ± 0.8823 fold;

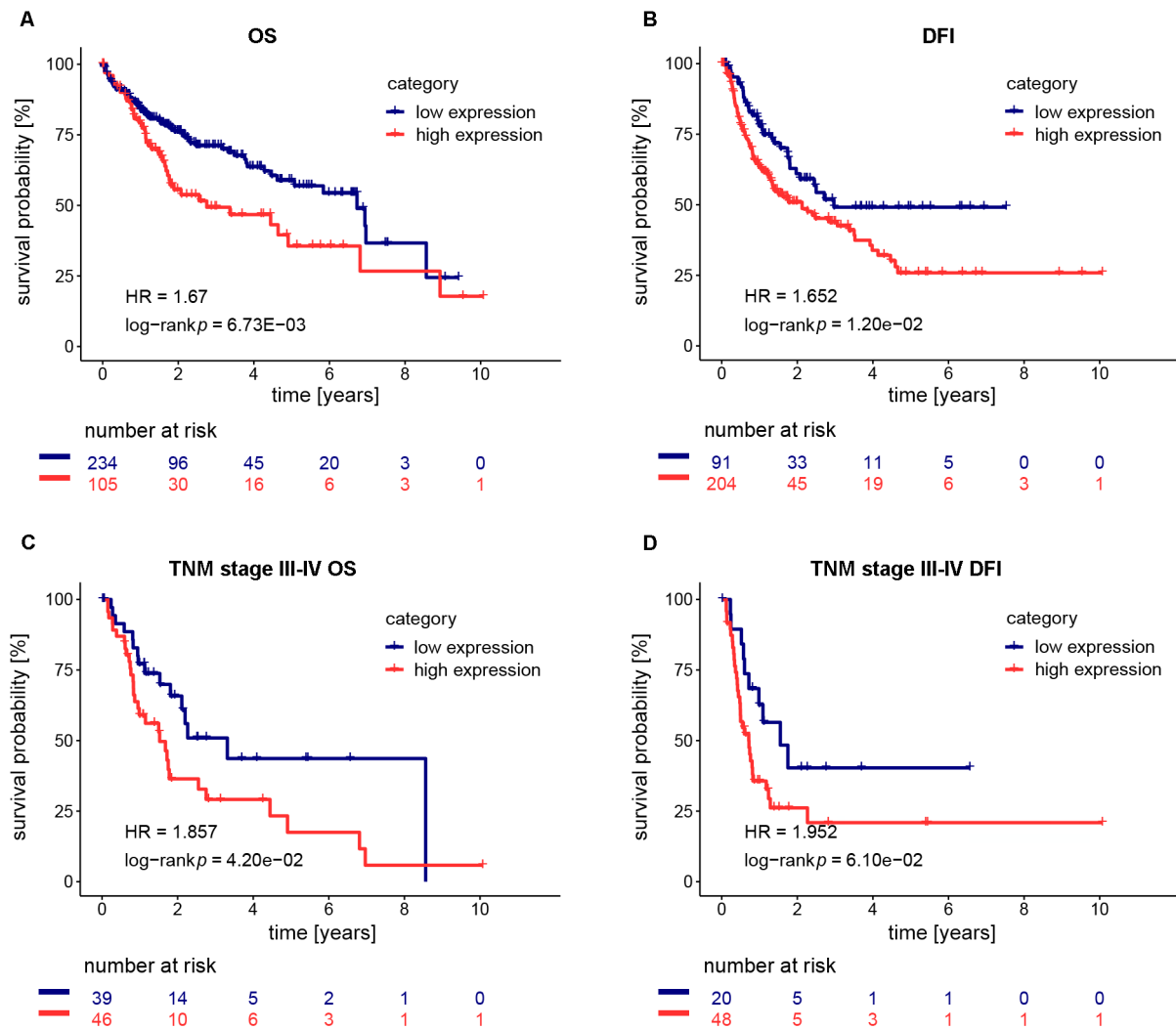


Fig. 3. Association between NME1 mRNA level and overall survival (OS) or disease-free interval (DFI). A,B. The Kaplan–Meier curve was used to analyze the correlation between NME1 mRNA levels and OS (A) or DFI (B) in patients with hepatocellular carcinoma (HCC); C,D. Analysis of OS (C) and DFI (D) based on mRNA levels of NME1 in patients with TNM stage III or IV of HCC. The log-rank test was used for statistical analysis (A–D)

HR – hazard ratio.

Huh7: 1.009 ± 0.1712 fold compared to 8.326 ± 0.5093 fold, $n = 3$, all $p < 0.0010$), and reduced the mRNA (Hep3B: 1.001 ± 0.0453 fold compared to 0.6030 ± 0.0430 fold; Huh7: 1.000 ± 0.0187 fold compared to 0.4484 ± 0.0271 fold, $n = 3$, all $p < 0.0010$) and protein (Hep3B: 1.000 ± 0.0251 fold compared to 0.4055 ± 0.0047 fold; Huh7: 1.000 ± 0.183 fold compared to 0.380 ± 0.020 fold, $n = 3$, all $p < 0.0001$) levels of NME1 (Fig. 6E,F). In contrast, miR-139-5p inhibitor did not change the level of miR-139-5p in HCC cells (Hep3B: 1.008 ± 0.1567 fold compared to 1.143 ± 0.1705 fold; Huh7: 1.029 ± 0.3149 fold compared to 1.349 ± 0.1209 fold, $n = 3$, all $p > 0.0500$), but enhanced the mRNA (Hep3B: 1.000 ± 0.0313 fold compared to 5.917 ± 0.5942 fold; Huh7: 1.001 ± 0.0527 fold compared to 6.160 ± 0.1128 fold, $n = 3$, all $p < 0.0010$) and protein (Hep3B: 1.000 ± 0.0102 fold compared to 1.314 ± 0.0391 fold; Huh7: 1.000 ± 0.103 fold compared to 1.960 ± 0.095 fold, $n = 3$, all $p < 0.0010$) levels of NME1 (Fig. 6E,F). Overall, miR-139-5p targets NME1 and downregulates its expression.

NME1 is associated with cell cycle, DNA replication, oxidative phosphorylation, and pentose phosphate pathways

To investigate the biological processes that may be regulated by NME1, we analyzed the genes co-expressed with NME1 using GSEA. These genes were found to be enriched in the gene sets for cell cycle, DNA replication, oxidative phosphorylation, and pentose phosphate pathways (Fig. 7). Genes related to these biological processes and co-expressed with NME1 are listed in Fig. 7.

miR-139-5p suppresses cellular proliferation by downregulating NME1

To confirm the conclusion of bioinformatics analysis, we investigated the effect of miR-139-5p/NME1 axis on cellular proliferation, using in vitro experiments. First, we overexpressed miR-139-5p or NME1 by transfection

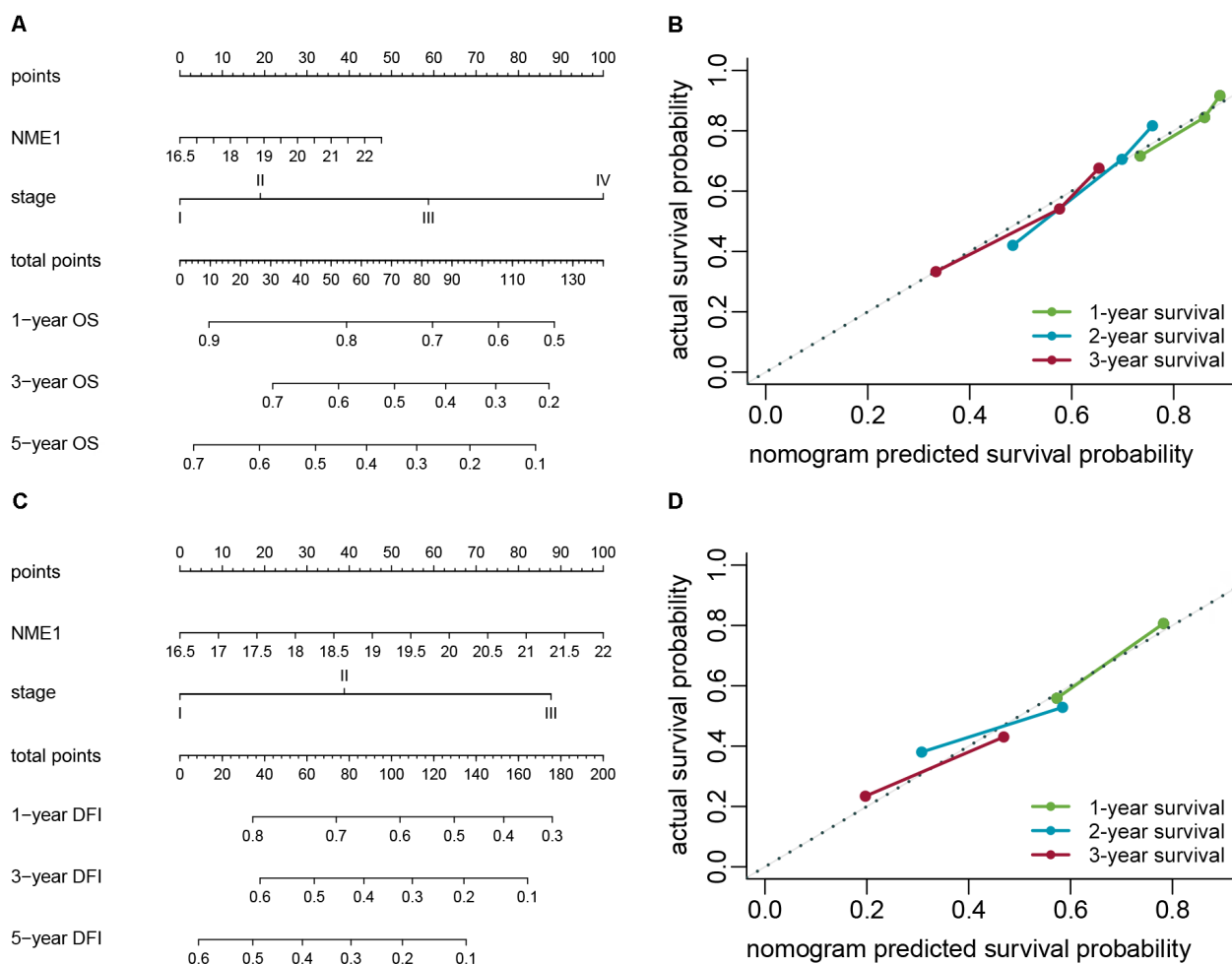


Fig. 4. Prognostic value of NME1 in hepatocellular carcinoma (HCC). A,B. Based on the expression level of NME1 and TNM stage, a prognostic nomogram (A) of HCC patients and a nomogram calibration curve (B) for predicting overall survival (OS) were plotted; C,D. Based on NME1 and TNM stage, a nomogram (C) and calibration curve (D) for patients with HCC for predicting disease-free interval (DFI) were plotted

with miR-139-5p mimic and NME1 OE plasmid, respectively. As shown in Fig. 8A, miR-139-5p mimic elevated the miR-139-5p level in Hep3B and Huh7 cells ($n = 3$, all $p < 0.0001$), and the NME1 OE plasmid had no significant effect on the level of miR-139-5p ($n = 3$, all $p > 0.0500$). Moreover, miR-139-5p mimic significantly decreased the mRNA (Fig. 8B, $n = 3$, all $p < 0.0500$) and protein (Fig. 8C, $n = 3$, all $p < 0.0500$) levels of NME1. In addition, the NME1 overexpression significantly rescued the miR-139-5p mimic-induced reduction in NME1 levels (Fig. 8B,C, $n = 3$, all $p < 0.0500$).

Next, the EdU assay was performed to determine the cell proliferation. As shown in Fig. 9A, the miR-139-5p mimic reduced the percentage of EdU⁺ cells (Hep3B: $77.0 \pm 2.7\%$ compared to $48.4 \pm 5.5\%$; Huh7: $54.6 \pm 2.8\%$ compared to $33.1 \pm 2.1\%$, $n = 3$, all $p < 0.0100$), indicating that miR-139-5p suppressed the cellular proliferation. Moreover, the NME1 overexpression relieved the inhibitory effect of miR-139-5p on cell proliferation (Hep3B: $49.3 \pm 4.1\%$ compared to $62.0 \pm 3.8\%$; Huh7: $31.9 \pm 2.6\%$ compared to $45.25 \pm 2.6\%$, $n = 3$, all $p < 0.0100$) (Fig. 9A). In addition, the miR-139-5p overexpression caused a cell-cycle arrest

at G₀/G₁ phase (Hep3B: $33.8 \pm 1.6\%$ compared to $51.5 \pm 1.7\%$; Huh7: $40.4 \pm 3.4\%$ compared to $56.1 \pm 0.5\%$, $n = 3$, all $p < 0.0100$), while NME1 overexpression alleviated the arrest induced by miR-139-5p (Hep3B: $51.7 \pm 2.3\%$ compared to $42.9 \pm 2.0\%$; Huh7: $55.2 \pm 0.7\%$ compared to $47.6 \pm 1.1\%$, $n = 3$, all $p < 0.0100$) (Fig. 9B).

Taken together, miR-139-5p inhibits cell growth by downregulating NME1 expression.

Discussion

The NME1 is a highly conserved multifunctional protein. Previous studies have shown that elevating NME1 levels inhibits the migration of various tumor cells, such as melanoma, breast cancer and prostate cancer.^{18,21,22} One study showed that the polymorphisms in the *NME1* gene are significantly associated with an increased susceptibility to gynecological cancer, decreased sensitivity to gastric cancer, increased susceptibility to non-small cell lung cancer, and reduced risk of cervical cancer.⁴ Furthermore, reducing the expression of NME1 protein promotes the growth and

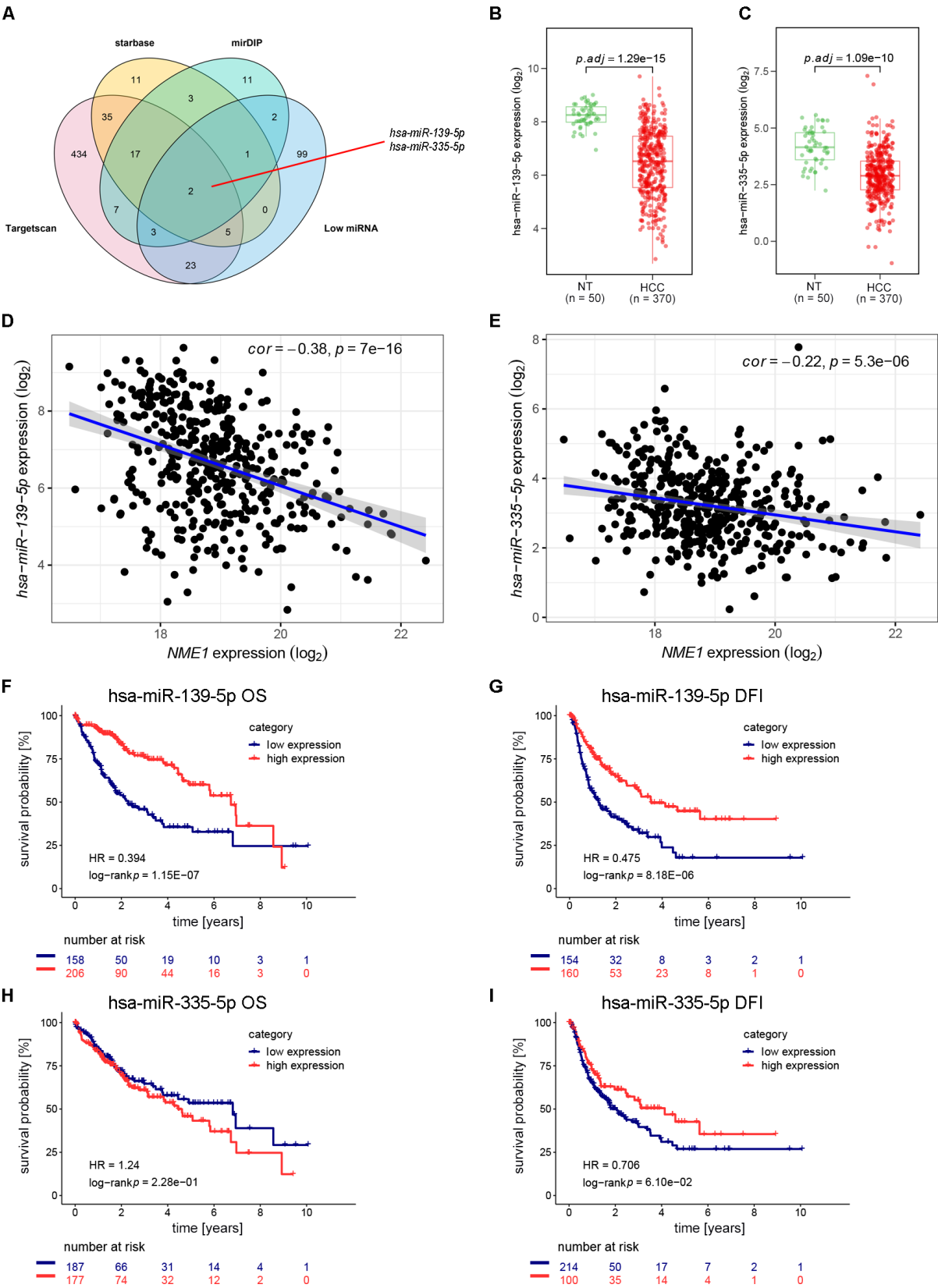


Fig. 5. The miR-139-5p and miR-335-5p are negatively correlated with NME1. A, Venn diagram; B,C, Comparison of miR-139-5p (B) or miR-335-5p (C) levels in hepatocellular carcinoma (HCC) tissues (n = 370) samples and normal tissues (NT) (n = 50) in the Cancer Genome Atlas liver hepatocellular carcinoma (TCGA-LIHC); D,E, The NME1 mRNA level was negatively correlated with *hsa-miR-139-5p* level (D) or *hsa-miR-335-5p* level (E); F–I, The Kaplan–Meier analysis showing the correlation of *hsa-miR-139-5p* level with overall survival (OS) (F) or disease-free interval (DFI) (G), and of *hsa-miR-335-5p* level with OS (H) or DFI (I). The Mann–Whitney test (B,C) and the log-rank test (F–I) were used for statistical analysis. Linearity curves and Kaplan–Meier curves were drawn based on the data from the TCGA

HR – hazard ratio.

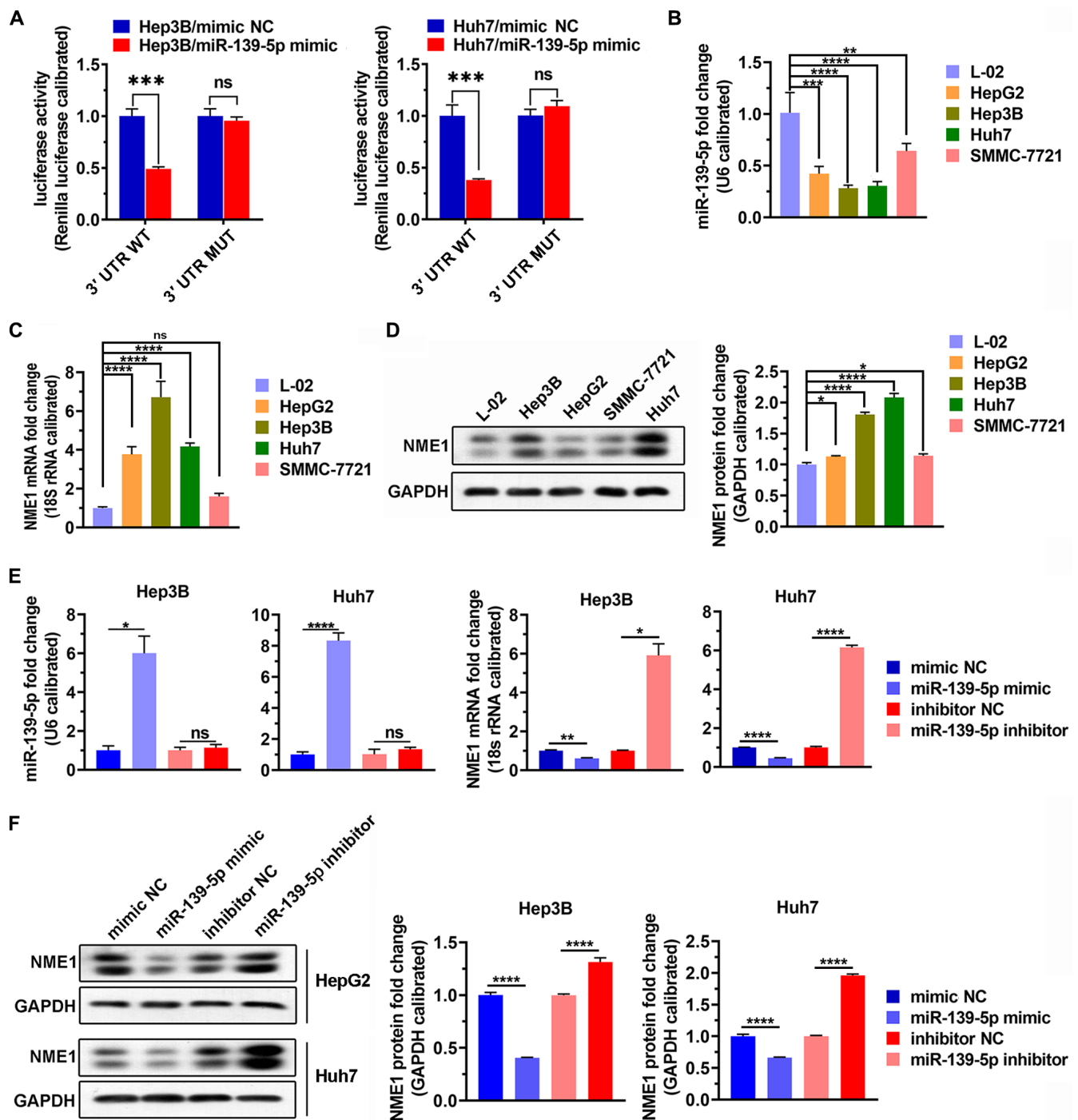


Fig. 6. The miR-139-5p suppresses the expression of NME1. **A.** A dual-luciferase reporter system was used to analyze the correlation between miR-139-5p and the 3' UTR of NME1; **B.** The miR-139-5p levels in cell lines were detected using quantitative reverse transcription polymerase chain reaction (qRT-PCR); **C.** The NME1 expression levels in cell lines were detected using qRT-PCR; **D.** Western blotting showing the NME1 protein level in cell lines; **E.** The NME1 mRNA levels were detected after transfection with miR-139-5p mimic and miR-139-5p inhibitor, respectively; **F.** The NME1 protein levels were detected after transfection with miR-139-5p mimic and miR-139-5p inhibitor, respectively. Data are presented as mean \pm standard deviation (SD) of 3 biological replicates. Data were analyzed using Student's t-test (A,E,F) and analysis of variance (ANOVA), followed by Tukey's post hoc test (B–D).

UTR – untranslated region; 3' UTR WT – wide-type *NME1* 3' UTR; 3' UTR MUT – mutant *NME1* 3' UTR; ns – no significance; * $p < 0.0500$; ** $p < 0.0100$; *** $p < 0.0010$; **** $p < 0.0001$.

lymph node metastasis of human breast cancer. However, enhancing the expression of NME1 reduces survival rates in patients with neuroblastoma. Increasing expression of NME1 in gastric cancer promotes distant metastasis of gastric cancer and reduces the 2-year disease-free

survival rate of patients.^{23,24} Bioinformatic analyses showed that NME1 levels in HCC tissues were higher than those in hepatitis, cirrhosis or normal liver tissues.¹⁸ The NME1 is highly expressed in colorectal cancer tissues and is tightly associated with the metastatic potential of colorectal

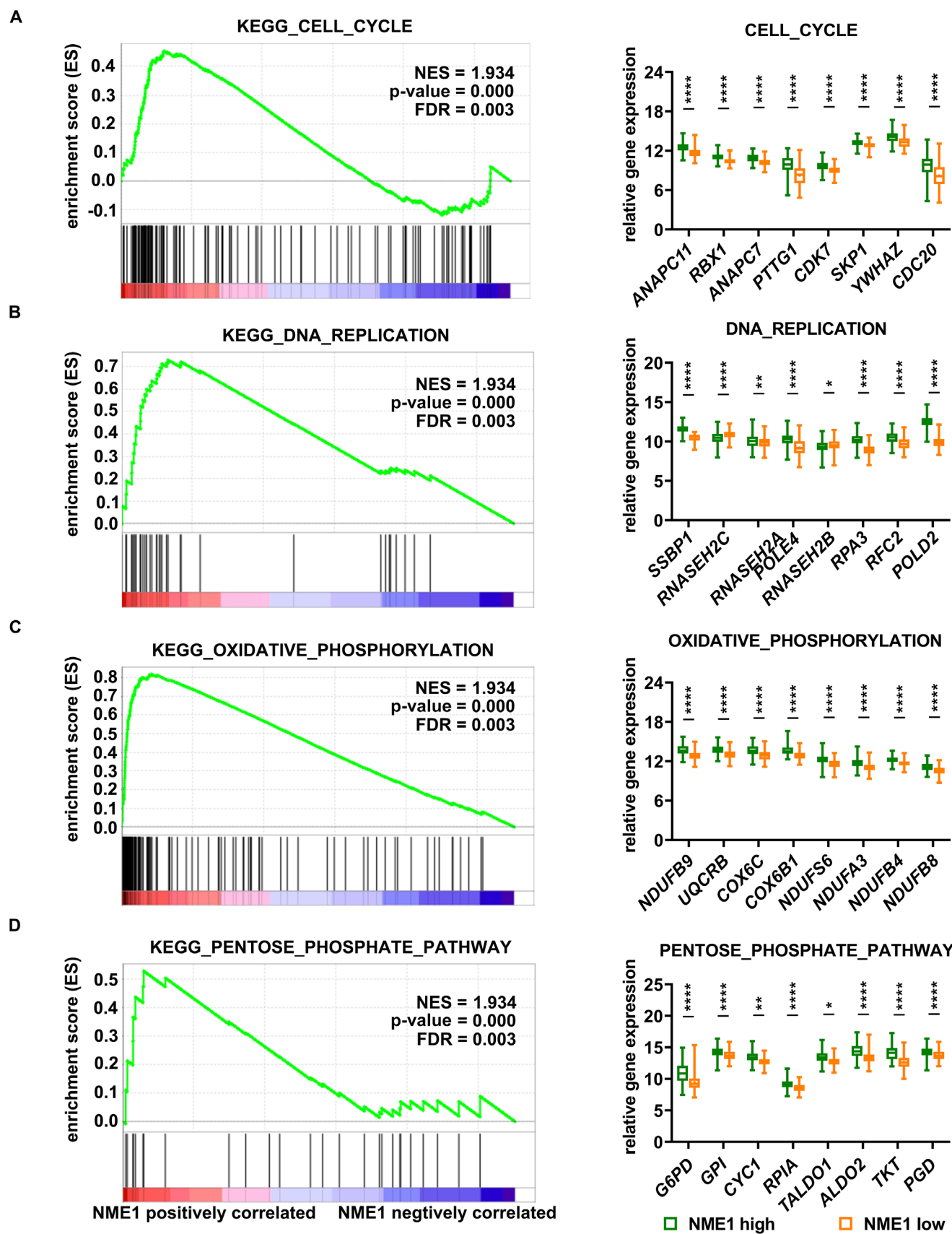


Fig. 7. Gene set enrichment analysis (GSEA) of potential biological functions of upregulated NME1 in hepatocellular carcinoma (HCC). A–D. The correlation between NME1 expression level and the cell cycle (A), DNA replication (B), oxidative phosphorylation (C) or pentose phosphate pathways (D), and the relationship between NME1 expression level and the expression of genes related to the 3 biological processes. The Mann–Whitney test was used to analyze the data (A–D)

KEGG – Kyoto Encyclopedia of Genes and Genomes; NES – normalized enrichment score; FDR – false discovery rate. *p < 0.05; **p < 0.01; ****p < 0.0001.

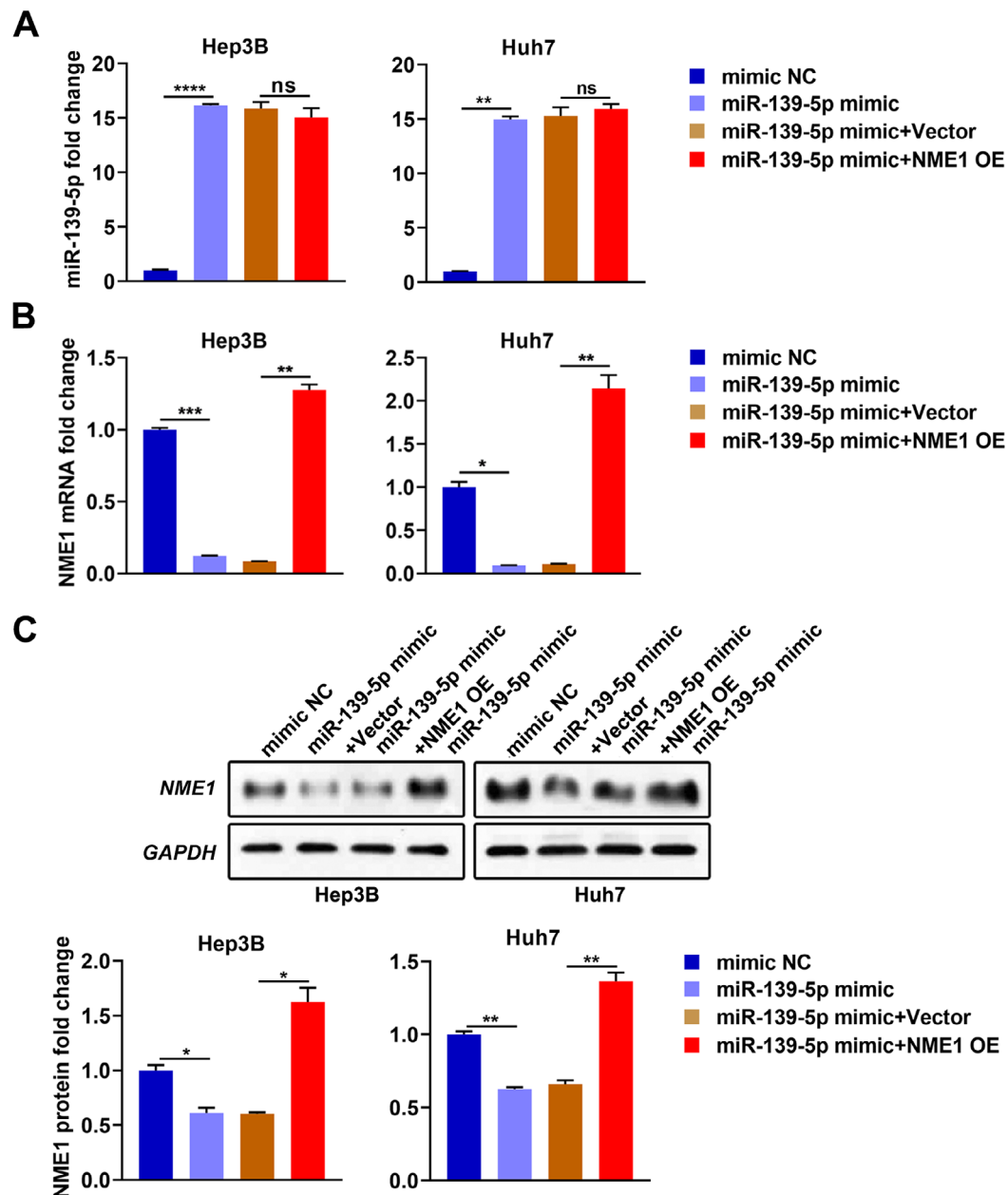


Fig. 8. The miR-139-5p inhibits cell proliferation by downregulating NME1. After miR-139-5p mimic was transfected alone or co-transfected with overexpressing NME1 (NME1 OE) plasmid into Hep3B and Huh7 cells, the levels of miR-139-5p (A), NME1 mRNA (B) and NME1 protein (C) were detected. Data are presented as mean \pm standard deviation (SD) of 3 biological replicates and analyzed using Student's t-test

ns – no significance; * $p < 0.05$; ** $p < 0.01$; *** $p < 0.001$; **** $p < 0.0001$.

cancer. The NEM1 is considered a prognostic factor for colorectal cancer.^{18,25} Our study revealed that NME1 was upregulated in HCC, and the level of NME1 was significantly correlated with the clinicopathological characteristics and prognosis. These findings indicated that NME1 has different functions in different tumors.

Mature miRNAs binds to the 3' UTR of targeting mRNA, resulting in the degradation of mRNAs or suppression of mRNA translation.^{26,27} Studies have shown that a single miRNA may participates in various pathophysiological processes, including cell proliferation, cell apoptosis, cell differentiation, and organ development by regulating

multiple potential targets, thereby promoting or inhibiting the progression of human cancer.^{26,28–30} The miR-139-5p, located on chromosome 11q13.4, inhibits the occurrence of esophageal cancer by regulating vascular endothelial growth factor receptor (VEGFR) signaling pathway,^{26,31,32} suppressing the growth and migration of osteosarcoma cells by regulating DNMT1,³³ promoting the invasiveness of adrenocortical carcinoma by targeting the downstream gene of N-myc,³⁴ and inhibiting the growth, metastasis and glycolysis of gallbladder cancer cells by downregulating PKM2.³⁵ In addition, serum miR-139-5p is considered an indicator of osteosarcoma.³⁶ In non-small cell

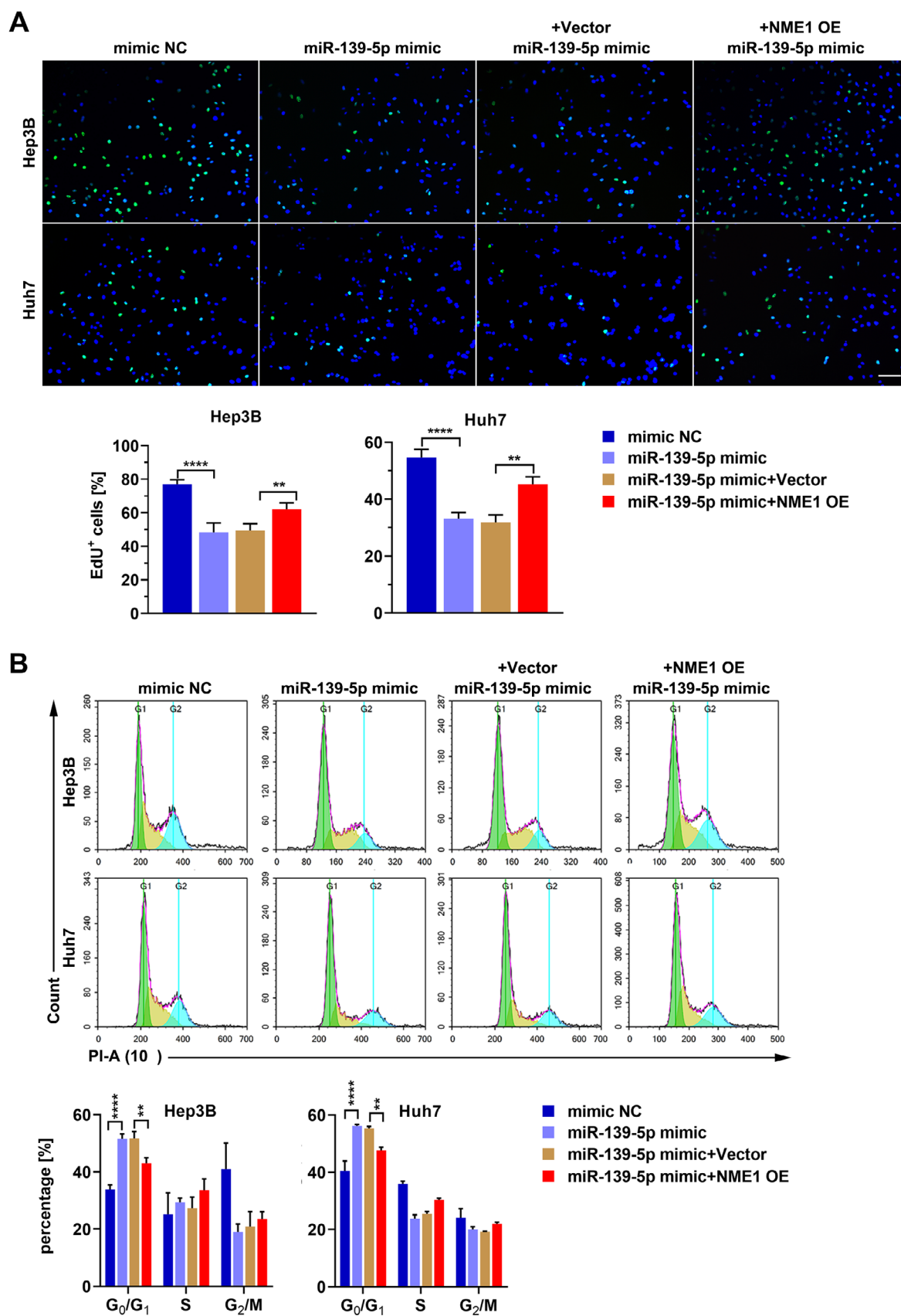


Fig. 9. The miR-139-5p inhibits cell proliferation by downregulating NME1. The cell proliferation was determined using EdU assay (A), and the cell cycle was analyzed with flow cytometry using propidium iodide (PI) staining (B). Data are presented as mean \pm standard deviation (SD) of 3 biological replicates and analyzed using Student's t-test

NME1 OE – overexpressing NME1; ** $p < 0.0100$; *** $p < 0.0010$; **** $p < 0.0001$.

lung cancer, the lncRNA AFAP1-AS1 inhibits miR-139-5p by upregulating RRM2 to promote cell proliferation.³⁷ The miR-139-5p, which is downregulated in HCC cells, inhibits the epithelial–mesenchymal transition of HCC cells.³⁸ According to previous studies, miR-139-5p may also suppress the deterioration of HCC by targeting multiple genes, such as *ZEB1*, *ZEB2*, *TCF-4*, *XIST1*, and *c-Fos*.^{30,38–40} Our study revealed that miR-139-5p negatively regulates the expression of NME1 in HCC cells. Our findings show that miR-139-5p may serve as a tumor suppressor in HCC.

Limitations


It should be noted that there are also several limitations to this study. The results of our GSEA analysis indicate that NME1 is related to cell cycle, DNA replication, oxidative phosphorylation, and pentose phosphate pathways. We confirmed that miR-139-5p downregulates NME1 to induce G₀/G₁ arrest and inhibit cellular proliferation. However, the underlying mechanism of miR-139-5p on regulating oxidative phosphorylation and pentose phosphate pathways by targeting NME1 needs to be studied further. Signaling pathways which are regulated by miR-139-5p/NME1 axis need to be determined. Moreover, we should study the effect of miR-139-5p/NME1 axis on cell apoptosis and metastasis in the next research. In addition, the antitumor activity of miR-139-5p should also be verified in vivo.


Conclusions


The NME1 is highly expressed in HCC tissues. Higher NME1 level indicates worse OS and DFI in patients with HCC. In contrast, miR-139-5p is lowly expressed in HCC tissues. Higher NME1 level indicates better OS and DFI. Furthermore, miR-139-5p targets NME1 3' UTR and suppresses cellular proliferation by downregulating NME1 expression.

ORCID iDs

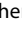
Jun Yang  <https://orcid.org/0000-0003-3942-433X>

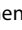
De Zhi Li  <https://orcid.org/0000-0002-4500-7439>

Yu Pang  <https://orcid.org/0000-0002-7457-8863>

Tao Zhou  <https://orcid.org/0000-0003-1547-0462>

Jia Sun  <https://orcid.org/0000-0002-1249-0030>

Xian Yi Cheng  <https://orcid.org/0000-0003-4265-6916>

Wei V. Zheng  <https://orcid.org/0000-0002-8942-1543>

References

1. Ferlay J, Soerjomataram I, Dikshit R, et al. Cancer incidence and mortality worldwide: Sources, methods and major patterns in GLOBOCAN 2012. *Int J Cancer*. 2015;136(5):E359–E386. doi:10.1002/ijc.29210
2. Zucman-Rossi J, Villanueva A, Nault JC, Llovet JM. Genetic landscape and biomarkers of hepatocellular carcinoma. *Gastroenterology*. 2015;149(5):1226–1239.e1224. doi:10.1053/j.gastro.2015.05.061
3. Nahon P, Zucman-Rossi J. Single nucleotide polymorphisms and risk of hepatocellular carcinoma in cirrhosis. *J Hepatol*. 2012;57(3):663–674. doi:10.1016/j.jhep.2012.02.035
4. Shi X, Jin H, Peng M, et al. Association between NME1 polymorphisms and cancer susceptibility: A meta-analysis based on 1644 cases and 2038 controls. *Pathol Res Pract*. 2018;214(4):467–474. doi:10.1016/j.prp.2018.02.020
5. Bilitou A, Watson J, Gartner A, Ohnuma S. The NM23 family in development. *Mol Cell Biochem*. 2009;329(1–2):17–33. doi:10.1007/s11010-009-0121-6
6. Dooley S, Seib T, Engel M, et al. Isolation and characterization of the human genomic locus coding for the putative metastasis control gene *nm23-H1*. *Hum Genet*. 1994;93(1):63–66. doi:10.1007/bf00218915
7. Xue R, Peng Y, Han B, Li X, Chen Y, Pei H. Metastasis suppressor NME1 promotes non-homologous end joining of DNA double-strand breaks. *DNA Repair (Amst)*. 2019;77:27–35. doi:10.1016/j.dnarep.2019.03.003
8. Chen J, Jiang Q, Jiang XQ, et al. miR-146a promoted breast cancer proliferation and invasion by regulating NM23-H1. *J Biochem*. 2020;167(1):41–48. doi:10.1093/jb/mvz079
9. Braun S, Mauch C, Boukamp P, Werner S. Novel roles of NM23 proteins in skin homeostasis, repair and disease. *Oncogene*. 2007;26(4):532–542. doi:10.1038/sj.onc.1209822
10. Kaetzel DM, Leonard MK, Cook GS, et al. Dual functions of NME1 in suppression of cell motility and enhancement of genomic stability in melanoma. *Naunyn Schmiedeberg's Arch Pharmacol*. 2015;388(2):199–206. doi:10.1007/s00210-014-1010-4
11. Puts GS, Leonard MK, Pamidimukkala NV, Snyder DE, Kaetzel DM. Nuclear functions of NME proteins. *Lab Invest*. 2018;98(2):211–218. doi:10.1038/labinvest.2017.109
12. Gao QL, Ma D, Meng L, et al. Association between *Nm23-H1* gene expression and metastasis of ovarian carcinoma. *Ai Zheng*. 2004;23(6):650–654. PMID:15191664.
13. Goncharuk VN, del-Rosario A, Kren L, et al. Co-downregulation of PTEN, KAI-1, and nm23-H1 tumor/metastasis suppressor proteins in non-small cell lung cancer. *Ann Diagn Pathol*. 2004;8(1):6–16. doi:10.1016/j.anndiagpath.2003.11.002
14. Kaetzel DM, McCorkle JR, Novak M, Yang M, Jarrett SG. Potential contributions of antimutator activity to the metastasis suppressor function of NM23-H1. *Mol Cell Biochem*. 2009;329(1–2):161–165. doi:10.1007/s11010-009-0108-3
15. Lagos-Quintana M, Rauhut R, Yalcin A, Meyer J, Lendeckel W, Tuschl T. Identification of tissue-specific microRNAs from mouse. *Curr Biol*. 2002;12(9):735–739. doi:10.1016/s0960-9822(02)00809-6
16. Bartel DP. MicroRNAs: Target recognition and regulatory functions. *Cell*. 2009;136(2):215–233. doi:10.1016/j.cell.2009.01.002
17. Almeida MI, Nicoloso MS, Zeng L, et al. Strand-specific miR-28-5p and miR-28-3p have distinct effects in colorectal cancer cells. *Gastroenterology*. 2012;142(4):886–896.e9. doi:10.1053/j.gastro.2011.12.047
18. Yang J, Lv Z, Huang J, Zhao Y, Li Y. High expression of NME1 correlates with progression and poor prognosis in patients of hepatocellular carcinoma. *Int J Clin Exp Pathol*. 2017;10(8):8561–8568. PMID:31966710.
19. Yu B, Ding Y, Liao X, Wang C, Wang B, Chen X. Overexpression of PARPBP correlates with tumor progression and poor prognosis in hepatocellular carcinoma. *Dig Dis Sci*. 2019;64(10):2878–2892. doi:10.1007/s10620-019-05608-4
20. Xu X, Zheng S. MiR-887-3p negatively regulates STARD13 and promotes pancreatic cancer progression. *Cancer Manag Res*. 2020;12:6137–6147. doi:10.2147/cmar.S260542
21. Steeg PS, Horak CE, Miller KD. Clinical-translational approaches to the Nm23-H1 metastasis suppressor. *Clin Cancer Res*. 2008;14(16):5006–5012. doi:10.1158/1078-0432.Ccr-08-0238
22. Li Y, Zhou Q, Sun Z, et al. Experimental study on molecular mechanism of *nm23-H1* gene transfection reversing the malignant phenotype of human high-metastatic large cell lung cancer cell line [in Chinese]. *Zhongguo Fei Ai Za Zhi*. 2006;9(4):307–311. doi:10.3779/j.issn.1009-3419.2006.04.01
23. Wang CS, Lin KH, Hsu YC, Hsueh S. Distant metastasis of gastric cancer is associated with elevated expression of the antimetastatic *nm23* gene. *Cancer Lett*. 1998;128(1):23–29. doi:10.1016/s0304-3835(98)00043-3
24. Müller W, Schneiders A, Hommel G, Gabbert HE. Expression of nm23 in gastric carcinoma: Association with tumor progression and poor prognosis. *Cancer*. 1998;83(12):2481–2487. doi:10.1002/(sici)1097-0142(19981215)83:12<2481::aid-cncr11>3.0.co;2-p
25. Kapitanović S, Cacev T, Berković M, et al. nm23-H1 expression and loss of heterozygosity in colon adenocarcinoma. *J Clin Pathol*. 2004;57(12):1312–1318. doi:10.1136/jcp.2004.017954

26. Jiao W, Zhang J, Wei Y, et al. MiR-139-5p regulates VEGFR and downstream signaling pathways to inhibit the development of esophageal cancer. *Dig Liver Dis.* 2019;51(1):149–156. doi:10.1016/j.dld.2018.07.017
27. Qin C, Huang RY, Wang ZX. Potential role of miR-100 in cancer diagnosis, prognosis, and therapy. *Tumour Biol.* 2015;36(3):1403–1409. doi:10.1007/s13277-015-3267-8
28. Gu DN, Huang Q, Tian L. The molecular mechanisms and therapeutic potential of microRNA-7 in cancer. *Expert Opin Ther Targets.* 2015;19(3):415–426. doi:10.1517/14728222.2014.988708
29. Li P, Xiao Z, Luo J, Zhang Y, Lin L. MiR-139-5p, miR-940 and miR-193a-5p inhibit the growth of hepatocellular carcinoma by targeting SPOCK1. *J Cell Mol Med.* 2019;23(4):2475–2488. doi:10.1111/jcmm.14121
30. Gu W, Li X, Wang J. miR-139 regulates the proliferation and invasion of hepatocellular carcinoma through the WNT/TCF-4 pathway. *Oncol Rep.* 2014;31(1):397–404. doi:10.3892/or.2013.2831
31. Corbetta S, Vaira V, Guarnieri V, et al. Differential expression of microRNAs in human parathyroid carcinomas compared with normal parathyroid tissue. *Endocr Relat Cancer.* 2010;17(1):135–146. doi:10.1677/erc-09-0134
32. Shen K, Mao R, Ma L, et al. Post-transcriptional regulation of the tumor suppressor miR-139-5p and a network of miR-139-5p-mediated mRNA interactions in colorectal cancer. *FEBS J.* 2014;281(16):3609–3624. doi:10.1111/febs.12880
33. Shi YK, Guo YH. MiR-139-5p suppresses osteosarcoma cell growth and invasion through regulating DNMT1. *Biochem Biophys Res Commun.* 2018;503(2):459–466. doi:10.1016/j.bbrc.2018.04.124
34. Agosta C, Laugier J, Guyon L, et al. MiR-483-5p and miR-139-5p promote aggressiveness by targeting N-myc downstream-regulated gene family members in adrenocortical cancer. *Int J Cancer.* 2018;143(4):944–957. doi:10.1002/ijc.31363
35. Chen J, Yu Y, Chen X, et al. MiR-139-5p is associated with poor prognosis and regulates glycolysis by repressing PKM2 in gallbladder carcinoma. *Cell Prolif.* 2018;51(6):e12510. doi:10.1111/cpr.12510
36. Zhou L, Ma X, Yue J, et al. The diagnostic effect of serum miR-139-5p as an indicator in osteosarcoma. *Cancer Biomark.* 2018;23(4):561–567. doi:10.3233/cbm-181744
37. Huang N, Guo W, Ren K, et al. LncRNA AFAP1-AS1 suppresses miR-139-5p and promotes cell proliferation and chemotherapy resistance of non-small cell lung cancer by competitively upregulating RRM2. *Front Oncol.* 2019;9:1103. doi:10.3389/fonc.2019.01103
38. Qiu G, Lin Y, Zhang H, Wu D. miR-139-5p inhibits epithelial-mesenchymal transition, migration and invasion of hepatocellular carcinoma cells by targeting ZEB1 and ZEB2. *Biochem Biophys Res Commun.* 2015;463(3):315–321. doi:10.1016/j.bbrc.2015.05.062
39. Mo Y, Lu Y, Wang P, et al. Long non-coding RNA XIST promotes cell growth by regulating miR-139-5p/PDK1/AKT axis in hepatocellular carcinoma. *Tumour Biol.* 2017;39(2):1010428317690999. doi:10.1177/1010428317690999
40. Fan Q, He M, Deng X, et al. Derepression of c-Fos caused by microRNA-139 down-regulation contributes to the metastasis of human hepatocellular carcinoma. *Cell Biochem Funct.* 2013;31(4):319–324. doi:10.1002/cbf.2902